JOURNAL OF THERMOPHYSICS AND HEAT TRANSFER
Vol. 10, No. 1, January–March 1996

# Evaporative Heat Transfer at the Evaporative Section of a Grooved Heat Pipe

Yasunori Kobayashi,* Syuji Ikeda,† and Masanao Iwasa†
*University of Tsukuba, Tsukuba, Ibaraki 305, Japan*

**Evaporative heat and mass transfer phenomena in the vicinity of the liquid meniscus edge in the evaporator of a groove heat pipe is investigated theoretically and experimentally. A theoretical model for simulating the phenomena is proposed, which consists of macro- and microregions. The former represents the part of the liquid meniscus region where conventional heat and mass transfer take place, whereas the latter is a narrow meniscus edge region close and contacted to the solid wall where transport phenomenon is affected by the intermolecular forces or disjoining pressure. The numerical results obtained for ammonia as a working fluid indicate that a large heat flux on the order of megawatt per square meters is transported in the narrow microregion, and accordingly more than one-third of the total heat energy supplied from outer surface is transported through the microregion that is less than one-hundredth of the total meniscus area. An optical measurement was conducted at the meniscus edge to confirm the existence of the thin nonevaporative liquid film and to identify its thickness on the order of several tens of nanometers. These magnitudes of nonevaporative film thickness can be explained by the proposed theory.**

## Nomenclature

$A$ = dispersion constant, kJ
$f$ = fugacity
$G$ = mass flow rate, kg/s
$g$ = gravity constant, m/s$^2$
$H$ = film thickness, m
$K$ = curvature, m$^{-1}$
$k$ = thermal conductivity, kJ/ms
$M$ = molecular mass, kg/mol
$n$ = refractive index
$P$ = pressure, Pa
$Q$ = heat flux, kJ/m$^2$ s
$R$ = gas constant, kJ/kgK, and reflected energy intensity of the laser beam
$T$ = temperature, K
$v$ = liquid velocity, m/s
$\alpha$ = accommodation coefficient
$\theta$ = refractive angle of laser light
$\lambda$ = latent heat, kJ/kg, and wavelength of the laser light
$\mu$ = viscosity, Pa s
$\rho$ = density, kg/m$^3$
$\sigma$ = surface tension, N/m

*Subscripts*
$i$ = liquid–vapor interface
$l$ = liquid
$s$ = solid or saturated condition
$v$ = vapor
vi = vapor at liquid–vapor interface
$w$ = wall
0 = reference position
1 = outer surface of the groove wall

Presented as Paper 94-2032 at the AIAA/ASME 6th Joint Thermophysics and Heat Transfer Conference, Colorado Springs, CO, June 20–23, 1994; received July 13, 1994; revision received June 15, 1995; accepted for publication Aug. 27, 1995. 

*Professor, Institute of Engineering Mechanics. Member AIAA.
†Graduate Student, Graduate School of Engineering.

## I. Introduction

A GROOVE heat pipe has been extensively developed since heat pipe technology was initiated in the early 1960s for space applications, and now becomes the most frequently used heat transport element for the thermal design of recent sophisticated spacecrafts, although its heat transport capability is not necessarily superior to the other types of wicked heat pipe. On the other hand, recent progress in heat pipe designs and fabrication processes has been requiring more accurate information on the phenomena occurring inside the heat pipe; such as local heat transfer rates at arbitrary axial positions, the effect of noncondensable gas, oscillations of the temperature field, liquid film stability,[1] etc. Among others, the detailed information on local heat transfer rates at the evaporator and condenser sections has become crucial to maximizing the overall heat transport capability of the heat pipe.

Many efforts have been devoted to identifying the overall thermal performance of a heat pipe in a unified manner[2–4] and to analyzing the condensing flow in the condenser section[5–7] in conjunction with noncondensable gas effects in it. Investigations of the evaporator section are relatively recent topics that have been discussed with emphasis on evaporation of the liquid film at the meniscus edge.[8–14] Most of these works are on the theoretical modeling of grooved heat pipes and/or thermosyphons, apparently due to their structural simplicity, and therefore, analytical tractability of the phenomena. The earlier work in this area was initiated by Derjaguin[9] and developed in the 1970s by Refs. 10–12. However, there is very little experimental evidence available to date to confirm the validity of these models, especially nonevaporative thin liquid film, except for rather indirect information by means of laser holographic interferometry.[12]

This article deals with theoretical and experimental investigations of local evaporative heat transfer in the meniscus region of the axial groove heat pipe. The significance of the theoretical analysis is firstly, the meniscus contour is not given a priori, but is determined as a part of the solution of the problem; and secondly, the effect of evaporating heat transfer is considered in the macroregion as well as in the microregion. The optical measurement conducted, on the other hand, is to validate the critical assumption introduced in the theory that a thin nonevaporative film is always formed on the solid surface that is exposed to the vapor environment. The film thick-

ness of ethanol liquid was measured on the heated copper plate placed in the specially fabricated vacuum container and its typical result is presented.

## II. Theoretical Consideration

A theoretical heat transfer model in the axial groove structure is illustrated in Fig. 1a, which was developed by one of the authors and is summarized in the literature.[15] Therefore, only the important points are cited here along with newly obtained numerical results.

In the process of theoretical consideration it is assumed that the free surface of a working liquid contained in the groove holds a concave meniscus, and that the meniscus region is subdivided into two portions of macro- and microregions, as schematically shown in Fig. 2. The macroregion covers almost the whole area of liquid field where conduction, convection, and evaporation from the free surface will take place. The theoretical idea in the microregion is based on the similar concept to those originally developed in Ref. 10 and has the following features:

1) This region represents a narrow area close to and contacting the solid surface, and heat transport is characterized by intermolecular forces or equivalent disjoining pressure between the liquid molecules and those of the solid wall.

2) It is assumed that there always exists a thin liquid film on the solid surface that is connecting smoothly to the liquid bulk meniscus. It is also assumed that we can define the border or the interline dividing the microregion into evaporative and nonevaporative regions, depending on the relative effect of disjoining pressure, as illustrated in Fig. 2b. The entire liquid flowfield together with the surrounding walls can be solved consistently by utilizing the unified formulation.

## III. Governing Equations

### A. Microregion

The evaporative heat flux $Q_{mic}$ in the microregion is determined from kinetic energy exchange between molecules of the vapor and the adjacent liquid film and is given by a kinetic theory of thermodynamic equilibrium as

$$Q_{mic} = \frac{\alpha\lambda}{\sqrt{2\pi R}}\left(\frac{P_{vi}}{\sqrt{T_i}} - \frac{P_v}{\sqrt{T_v}}\right) \tag{1a}$$

where $P_{vi}$ and $P_v$ represent vapor pressures at the vapor–liquid interface and in the vapor field far from the liquid–vapor interface, respectively. Assuming the liquid and the vapor temperature at the interface are approximated in equilibrium thermodynamic state, the average temperature $\bar{T}$ ($\sqrt{\bar{T}} \cong \sqrt{T_i} \cong \sqrt{T_v}$) is introduced, so that we approximate Eq. (1a) as

$$Q_{mic} = \frac{\alpha\lambda}{\sqrt{2\pi R\bar{T}}}(P_{vi} - P_v) = \frac{\alpha\lambda}{\sqrt{2\pi R\bar{T}}}\Delta P \tag{1b}$$

where $\Delta p = p_{vi} - p_v$ represents a pressure difference in the vapor environment. The value of $\Delta p$ can be obtained from liquid state fugacity in thermodynamic relations[11] as

$$\mathrm{d}\,\overline{\ln} f_l = \frac{1}{R\rho_l T_l}\mathrm{d}p_l + \frac{\lambda}{RT_l^2}\mathrm{d}T_l \tag{2}$$

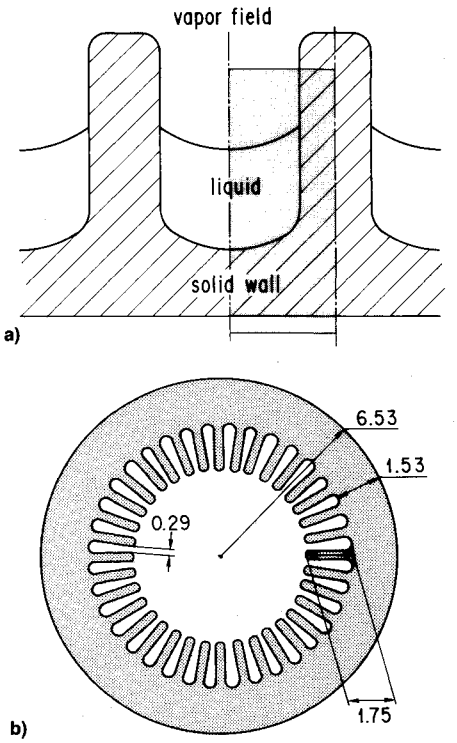


**Fig. 1 Cross-sectional view of the in-house groove heat pipe and its dimensions: a) schematic layout of groove section for analysis and b) cross-sectional configuration of actual heat pipe.**

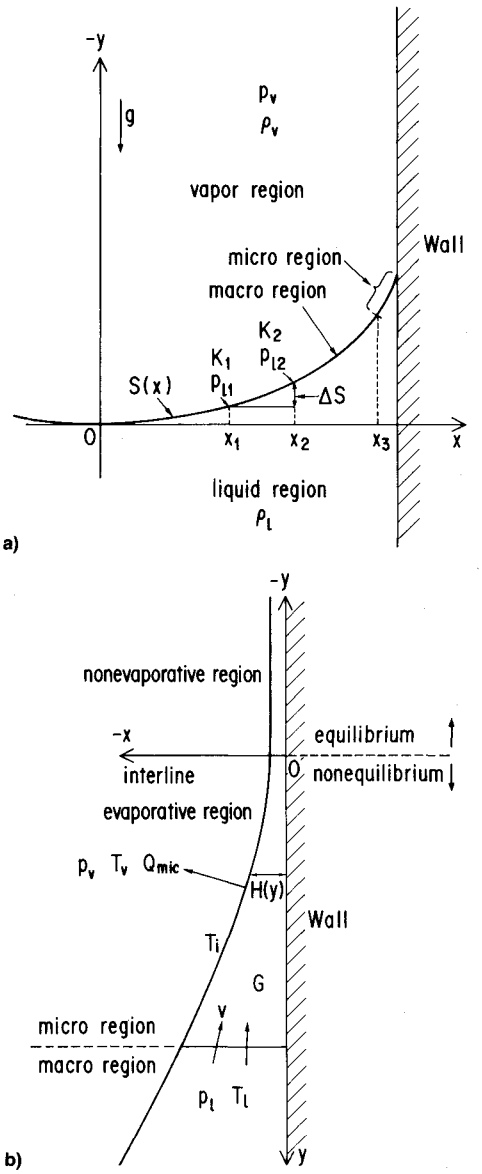


**Fig. 2 Theoretical modeling of meniscus; coordinate system and major parameters: a) macroregion and b) microregion.**

By integrating Eq. (2) in the vicinity of vapor–liquid interface where $f_l$ can be approximated as the vapor pressure $p_l$, we obtain the following relation:

$$\int \mathrm{d}\,\textit{//}\, f_l = \int_{p_v}^{p_{vi}} \mathrm{d}\,\textit{//}\, p_i = \int_{p_v}^{p_l} \frac{\mathrm{d}p}{R\rho_l T_i} + \int_{T_v}^{T_i} \frac{\lambda\,\mathrm{d}T}{RT^2}$$

$$\text{or} \quad \textit{//}\, \frac{p_{vi}}{p_v} = \frac{\lambda(T_i - T_v)}{RT_vT_i} + \frac{p_l - p_v}{R\rho_l T_i} \tag{3}$$

When we assume small differences in $p_{vi}$ and $p_v$, or $\textit{//}\, p_{vi}/p_v = (p_{vi} - p_v)/p_v$ is incorporated, the heat flux $Q_{mic}$ is rewritten as

$$Q_{mic} = \frac{\alpha\lambda^2\rho_v}{T_i\sqrt{2\pi R\bar{T}}}\left[(T_i - T_v) + \frac{T_v}{\lambda\rho_l}(p_l - p_v)\right] \tag{4}$$

In the nonevaporative region where the intermolecular force is dominant under a thermodynamic equilibrium condition, the disjoining pressure $p_d$ can be defined as the pressure difference between $p_v$ and $p_l$ and is expressed inversely proportional to $H$ to the third as

$$p_d = p_l - p_v = (A/H^3) \tag{5}$$

where $A$ is a measure of the intermolecular force between two interacting media. On the other hand, from the hydrostatic balance of liquid mass on the wall, the relation of film thickness and liquid density for $P_d$ in the microregion is derived as

$$\frac{\mathrm{d}p_d}{\mathrm{d}y} = \rho_l g, \quad \text{or} \quad \frac{\mathrm{d}H}{\mathrm{d}y} = \frac{\rho_l g H^4}{3A} \tag{6}$$

This relation is used to determine the contour of the liquid film $H(y)$ at arbitrary positions in the $y$ direction, starting from the position at interline $H(0)$ ($=H_0$, Fig. 2b), where $H_0$ is given from Eq. (4) by substituting $Q_{mic} = 0$ and assuming $T_i = T_w$ as

$$H_0 = \left[\frac{AT_v}{\rho_l\lambda(T_w - T_v)}\right]^{1/3} \tag{7}$$

Liquid mass evaporating from the film surface in the evaporative region (Fig. 2b) shall be supplied from the macroregion. When we assume the liquid flow in the evaporative region as pseudo-one-dimensional, conservation equations for mass and momentum are easily solved under boundary conditions of 1) nonslip condition at the wall: $v = 0$ at $x = 0$ and 2) no-shear stress at the free surface: $\mathrm{d}v/\mathrm{d}x = 0$ at $x = H$, to give the flow velocity $v$ in the evaporative microregion as

$$v = \frac{1}{\mu_l}\left(\frac{\mathrm{d}P_l}{\mathrm{d}y} - \rho_l g\right)\left(\frac{x^2}{2} - Hx\right) \tag{8}$$

From the law of mass conservation, the gross mass flow rate $G$ passing through the film at $H(y)$ with a unit width shall be balanced with the evaporating mass rate $Q_{mic}/\lambda$ from the film surface encompassing from the interline up to $y$ position, we obtain

$$G = \int_0^{H(y)} \rho_l v\,\mathrm{d}x = \int_0^y \left(\frac{Q_{mic}}{\lambda}\,\mathrm{d}y\right) \tag{9}$$

Further, we can assume that $\mathrm{d}p_v/\mathrm{d}y$ is negligibly small compared with $\mathrm{d}p_l/\mathrm{d}y$, so that we obtain from Eq. (5) as

$$\frac{\mathrm{d}p_l}{\mathrm{d}y} = \frac{\mathrm{d}p_d}{\mathrm{d}y} = \frac{3A}{H^4}\dot{H} \tag{10}$$

where the dot ($\cdot$) on the symbol $H$ denotes differentiation with respect to $y$. Accordingly, after differentiation of Eq. (9) and substitution of Eqs. (4), (6), (7), and (10) into it, the final form of $H(y)$ is arranged as

$$\ddot{H} = \frac{\mu_l\alpha\lambda\rho_v}{\rho_l AT_i\sqrt{2\pi R\bar{T}}}\left[(T_i - T_v) - \frac{T_vA}{\lambda\rho_l H^3}\right]H + \frac{\rho_l g H^3}{A}\dot{H} + \frac{\dot{H}^2}{H} \tag{11}$$

Equation 11 is solved by means of numerical integration (Runge–Kutta method).

### B. Macroregion

The free surface configuration $S(x)$ in the macroregion can be obtained from the hydrostatic balance of $\sigma$ and gravity force $\rho_l g$, as illustrated schematically in Fig. 2a. The origin in this figure represents a centerline of the groove symmetry, where the meniscus has a value of $\mathrm{d}S/\mathrm{d}x = 0$, and $x_3$ shows a border to the microregion where the gradient $\mathrm{d}S/\mathrm{d}x$ and its derivative $\mathrm{d}^2S/\mathrm{d}x^2$ should be equal to those given at the edge of the microregion to satisfy a smooth connection of both $S(x)$ and $H(y)$ curves on that point. Near the liquid surface at two arbitrary positions of $x_1$ and $x_2$ ($x_1$, $x_2 < x_3$), the following hydrostatic balance is maintained among the pressure, surface curvature, surface tension, and liquid density.

*1. Balance of Hydrostatic Force*

$$p_{l,2} - p_{l,1} = \rho_l g\Delta S, \quad \text{or} \quad \frac{\mathrm{d}p}{\mathrm{d}S} = \rho_l g \tag{12}$$

*2. Balance of Force at the Liquid–Vapor Interface*

$$p_v - p_{l,1} = \sigma K_1, \qquad P_v - P_{l,2} = \sigma K_2 \quad \text{or} \quad \mathrm{d}p = \sigma\,\mathrm{d}K \tag{13}$$

Consequently, the following relation is derived at an arbitrary position $x$ ($x < x_3$):

$$K' = (\rho_l g/\sigma)S' \tag{14}$$

where the symbol ($'$) denotes differentiation with respect to $x$, and therefore, $K$ has a general relation with $S$ as

$$K = S''/(1 + S'^2)^{3/2} \tag{15}$$

Finally, the relation of $S$ with respect to $x$ is summarized as

$$S''' - \frac{3S'S''^2}{(1 + S'^2)} - \left(\frac{\rho_l g}{\sigma}\right)S'(1 + S'^2)^{3/2} = 0 \tag{16}$$

where the boundary conditions are

$$\begin{gathered} S = S' = 0 \quad \text{at} \quad x = 0 \\ S' = 1/\dot{H}, \qquad S'' = 1/\ddot{H} \quad \text{at} \quad x = x_3 \end{gathered} \tag{17}$$

We solve Eq. (16) numerically under the restrictions of Eqs. (17) to determine the free surface contour $S(x)$ in the macroregion. The heat flux transported from the meniscus surface by evaporation can be obtained from Eqs. (4) and (13) as

$$Q_{mac} = \frac{\alpha\lambda^2 P_v}{T_i\sqrt{2\pi R\bar{T}}}\left[(T_i - T_v) - \frac{T_v}{\lambda\rho_l}(\sigma K)\right] \tag{18}$$

Figure 3 shows a numerical flowfield and adjacent solid walls (dotted area) representing schematically a cross-sectional area of the groove structure. A convective motion of

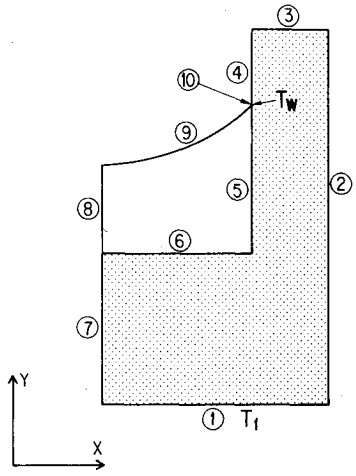


**Fig. 3 Schematic flowfield at groove section and its boundaries.**

the bulk liquid associated with heat transfer in the macroregion shall formally be described by three conservation equations. In the present study, however, we neglect any liquid bulk motion in this region in spite of the premise of allowing liquid mass flowing into the microregion as well as evaporation from the meniscus surface in the macroregion. The reason for neglecting this is to clarify whether such a narrow microregion has a significant role on the total heat transfer rates in the groove and to avoid computational complexities of solving velocity field that will give a minor effect on the heat transport problem discussed. This static–liquid assumption in the macroregion would practically correspond to a moderate heat-transport operating condition of the groove heat pipes. In this consequence the entire temperature field of the liquid and the surrounding solid walls can be expressed by Laplace equation as

$$\frac{\partial^2 T}{\partial x^2} + \frac{\partial^2 T}{\partial y^2} = 0 \tag{19}$$

which is solved numerically so as to satisfy the combining conditions between the macro- and microregions as expressed in Eq. (17) after postulating the following nine boundary conditions of ①–⑨, which are corresponding to encircled numbers in Fig. 3:

$T_1 = T_s = \text{const (given)}$ at boundary ①

$\dfrac{dT_i}{dn_i} = 0$ $(i = 2, 3, 4, 7, 8)$ at boundaries ②, ③, ④, ⑦, ⑧

$k_l \dfrac{dT_{li}}{dn_i} = k_s \dfrac{dT_{si}}{dn_i}$ $(i = 5, 6)$ at boundaries ⑤, ⑥

$-k_l \dfrac{dT_{19}}{dn_9} = Q_{\text{mac}}$ at boundary ⑨

where $n$ denotes a normal direction to the boundary surface. It should be noted that heat transportation is considered by way of liquid evaporation at the rate expressed in Eq. (18) from the liquid–vapor interface (the boundary ⑨) as well as by thermal conduction in the macroregion. The number ⑩ in Fig. 3 indicates a node representing a microregion with negligibly small scale in the figure where the heat flux $Q_{\text{mic}}$ flows out into the vapor atmosphere.

The numerical calculation was conducted using a finite difference technique, a Runge–Kutta method for solving differential equations. A successive overrelaxation (SOR) method is applied for numerical convergence for overall as well as for combining the processes of the two meniscus contours. The major flow of calculation process is as follows:

1) After storing necessary input data such as thermal properties of the substance and presumed values of operating vapor temperatures $T_v$ and the outer surface of the solid wall $T_1$, an arbitrary value is given to the wall temperature $T_w$ in the microregion or at the boundary ⑩.

2) The microregion is calculated first to determine the meniscus contour $H(y)$ by using Eq. (11) to an extent in the $y$ direction until no numerical convergence is maintained.

3) The meniscus contour in the macroregion is solved (as a boundary-value problem) from Eq. (16) together with connecting conditions of Eq. (17), starting from the contour edge in the microregion determined in process 2.

4) Once the meniscus contour is solved, the curve-linear coordinates system is generated to calculate the heat amount transferred in the entire macroregion.

5) Examine if the total heat energy transferred through the micro- and the macroregions equals the heat input from outside the solid surface (boundary ① in Fig. 3). If not equaled, the whole calculation process shall be repeated from process 2 after making a slight change in the value of $T_w$ until both amounts are equaled.

Practical calculation was performed to simulate heat transport capability of an in-house groove heat pipe filled with ammonia as working fluid, the overall thermal performance of which had been measured in our laboratory. The container of the heat pipe is made of aluminum alloy configured with 36 axial grooves or fins approximately 0.29 mm in width and 1.75 mm in height inside the tube by extrusion process. Its cross-sectional view and typical dimensions are illustrated in Fig. 1b. In the analysis, these groove configurations and its typical operating temperatures of $T_v$, $T_w$, and $T_1$ realized in the experiment were used as input data. Two kinds of working fluids, i.e., ammonia and ethanol, were examined. The analysis for ethanol fluid was conducted in order to compare the result with that of the meniscus experiment, as described in the next paragraph. Typical physical properties and operating conditions used in the calculation were tabulated in Table 1, where $A$ is a best engineering guess based on the information and data from other fluids.[11] The effect of $A$ on the heat flux was numerically examined by changing the value up to two orders of magnitude and the error was found to be of the order of 10% at most.

An approximate computer time required for converging the numerical result within less than 1% for typical heat transfer case was varied from 2 to 4 h using a recent model of an engineering workstation with a CPU speed of 100 mega-flops per second (MFP).

**Table 1 Physical properties[16] and constants used in calculation**

| Property | Liquid | |
|---|---|---|
| | Ammonia | Ethanol |
| $A$ | $2 \times 10^{-23}$ | $2 \times 10^{-23}$ |
| $\rho_l$ | 600.3 | 783.5 |
| $\rho_v$ | 8.233 | 0.1634 |
| $\sigma$ | 0.02013 | 0.022119 |
| $k_l$ | 0.4768 | 0.1660 |
| $\mu_l$ | $1.406 \times 10^{-4}$ | $1.405 \times 10^{-3}$ |
| $R$ | 0.4882 | 0.1805 |
| $P_v$ | $1.062 \times 10^{6}$ | $8.85 \times 10^{3}$ |
| $T_v$ | 300 | 300 |
| $T_w$ | 300.6 | 300.6 |
| $T_1$ | 301 | 301 |

## IV. Experiment

Optical measurements of liquid film thickness at the meniscus edge were conducted to examine the validity of the

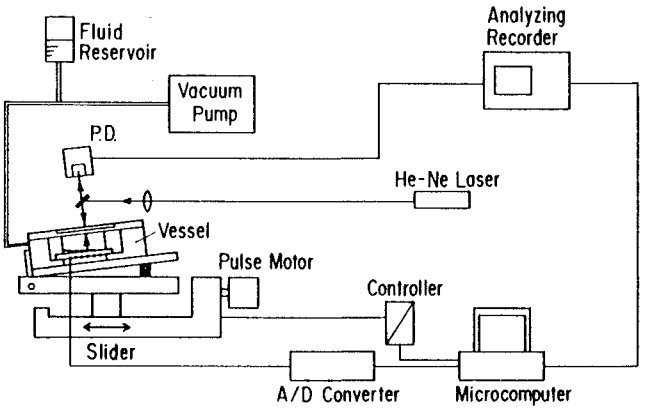


**Fig. 4 Schematic layout for film thickness measurement.**

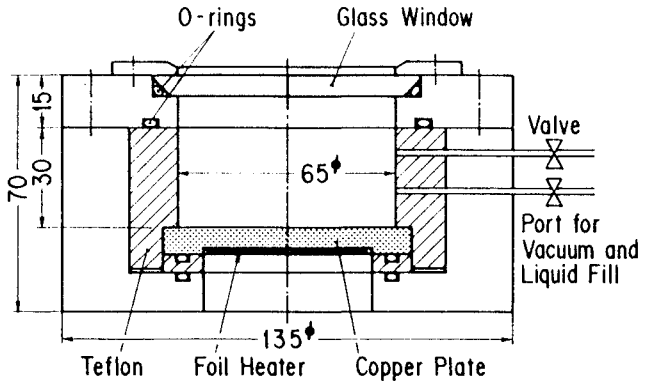


**Fig. 5 Rough drawing of test vessel for film thickness measurement.**

nonevaporative-liquid-film assumption in the microregion in the proposed theory. Figure 4 shows a schematic layout of the experimental apparatus. The test vessel specifically fabricated for meniscus measurement is mounted on the three-directional slider (or traversing bench). The slider is capable of positioning the vessel in an arbitrary attitude angle from vertical to horizontal and is able to move back and forth as far as 35 mm with positioning precision of 0.1 $\mu$m by the pulse motor-driving mechanism. The test vessel is made of bronze, having a cylindrical vacuum cavity of 135 mm in o.d. and 70 mm in height, as shown in Fig. 5. A heat-treated copper plate surface of 65 mm in diameter and 5 mm in thickness is installed in the vessel. The plate is thermally insulated from the surrounding vessel wall and is backed with foil heater to apply joule heating from its back. When a certain amount of working liquid is charged in the vessel a thin liquid film is naturally formed on the inclined copper plate by capillary force near the liquid contact edge. Laser light from a 30-mW continuous wave (CW)-type He–Ne laser source was injected 2.5 deg inclined from the normal to the copper plate while the slider is moved minutely so that the light beam is able to traverse the position on the copper surface perpendicular to the meniscus contact line. Two kinds of reflected beam energy $R$ were measured by traversing the laser beam on the same position on the copper plate; one is the energy reflected from the solid surface before ethanol is charged and the other is the multireflected beam energy between surfaces of the liquid film and solid surface after the liquid charge. The data detected by the photomultiplier detector (P.D.) were stored in the personal computer in the form of digitized signal to be processed in off-lines. The film thickness $\delta$ was calculated from the following optical relation as:

$$R = |r|^2 = \frac{r_{sl}^2 + r_{lv}^2 + 2r_{sl}r_{lv}\cos 2\beta}{1 + (r_{sl}r_{lv})^2 + 2r_{sl}r_{lv}\cos 2\beta} \tag{20}$$

where

$$\beta = 2\pi n_l \delta \cos\theta_l/\lambda$$
$$r_{sl} = \frac{\tan(\theta_s - \theta_l)}{\tan(\theta_s + \theta_l)}, \qquad r_{lv} = \frac{\tan(\theta_s - \theta_v)}{\tan(\theta_s + \theta_v)} \tag{21}$$

In the previous relations, $n_l$ is a refractive index of liquid at beam wavelength $\lambda$, and $\theta_s$, $\theta_l$, and $\theta_v$ are refractive angles for solid (copper plate), liquid film, and vapor, respectively, and are given from experimental conditions. The values of $R$ are the only measured data for calculating the film thickness. Measurements of film thickness in the vicinity of the meniscus edge were made extensively on ethanol for different heating rates on the copper plate under its pure vapor, but ammonia has not been examined due to safety reasons in handling this fluid in the laboratory.

## V. Results and Discussion

### A. Theoretical Results

Typical numerical results for meniscus configurations and heat transfer rates in the microregion of a groove configuration illustrated in Fig. 1b are shown in Fig. 6a and 6b for ammonia and ethanol, respectively, as a function of $\alpha$. In the figure, the origin of the abscissa stands for the interline representing the border of evaporative and nonevaporative liquid film in the theoretical model, as indicated in Fig. 2b. According to these numerical results, nonevaporative film thicknesses are in the order of few nanometers and are not affected largely by the value of $\alpha$. In addition, it is characteristic that heat transfer rates have a rapid increase in a narrow region of less than 1 $\mu$m in width followed by a rapid decrease owing to a strong cooling effect of evaporation in the meniscus, and that the maximum heat transfer rate occurs at the position

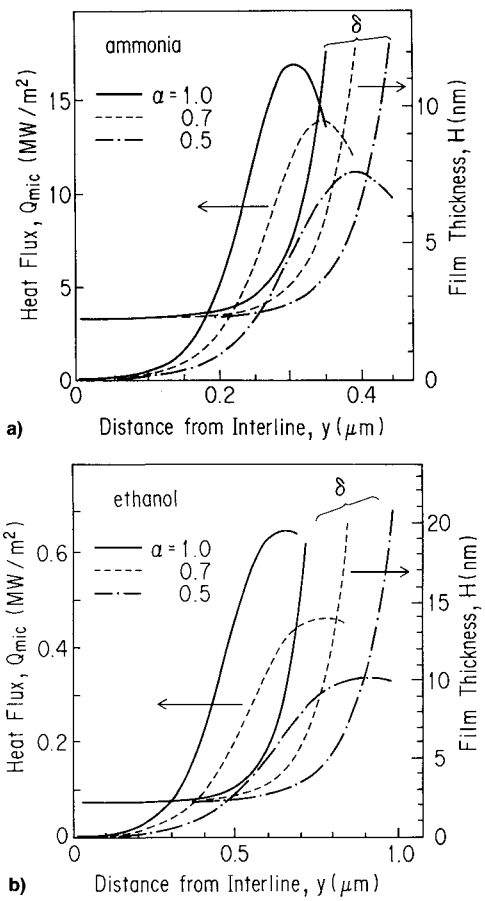


**Fig. 6 Liquid film thickness and heat transfer rates in the microregion for different values of $\alpha$.**

where the film thickness initiates a sharp increase, i.e., at the largest meniscus curvature. The notice here is that it is extremely difficult to identify the value $\alpha$ a priori, and therefore, some appropriate value has to be introduced in the calculation. Validity of the value $\alpha$ must be evaluated from experiment, which is another topic here. It was also found that the temperature difference $\Delta T$ $(= T_i - T_v)$ cannot be an independent variable and shall be determined in the process of solving the problem so as to satisfy energy conservation in the system. In the present numerical conditions of Table 1, $\Delta T$ was determined to be 0.00159 K.

Typical liquid meniscus contours or variation of film thickness in the microregion in the case of $\alpha = 1.0$ and $\Delta T = 0.00159$ K is shown in Fig. 7, after the two curves of $H(y)$ and $S(x)$ make a smooth connection to each other, satisfying the conditions of Eq. (17). This apparent smooth meniscus contour may raise the question of what the realistic contact angle of the meniscus is. Examining the meniscus profile in the figure, however, it must reasonably be approximated as the angle encompassing the wall surface and the line of linear extrapolation of the contour extended from the macroregion side.

Figure 8 shows typical temperature distributions of ammonia fluid in the macroregion corresponding to thermal conditions of Table 1 (ammonia), where the temperature increment between isothermal (dotted) lines is approximately 0.218 K. Figure 9 shows variation of the heat flux transferred from the macro and microregions for the corresponding thermal condition, which is illustrated in the different vertical scales. The dashed line in the figure is the authors' speculation; it would need another laborious calculation to combine this numerical grid distance by arranging finer mesh size. It is evident in the microregion that a huge heat flux on the order of megawatt per square meter ($MW/m^2$) is generated, and that it changes drastically in the narrow region. It was also found that the direction of gravity force gives only a slight effect on the heat flux distribution of Fig. 9, indicating that all grooves in Fig. 1b will work out equally as a heat transfer element. Table 2 summarizes ratios of the heat energy transferred through the microregion to the total heat input from the outer surface of the groove obtained for the operating conditions of Table 1 (ammonia). They indicate the significance of the microregion in evaporative heat transfer in the groove structure, as similarly pointed out in Ref. 14. According to the similar calculation for ethanol [for conditions of Table 1 (ethanol)], however, the role of the microregion becomes less significant when several percent of the total heat input is transferred.

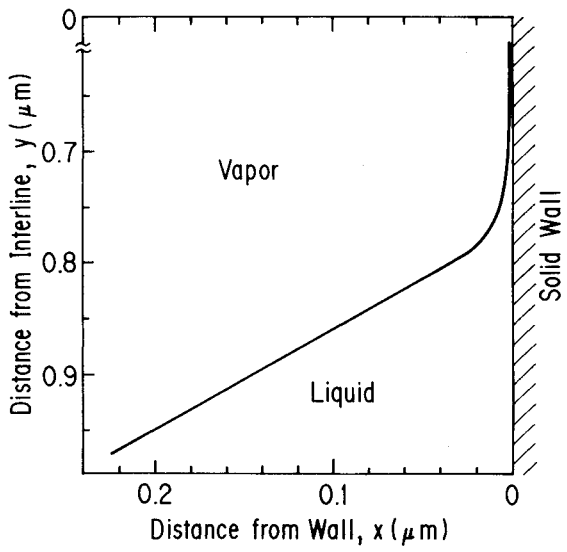


**Fig. 7 Typical numerical meniscus contours in the microregion of ammonia.**

**Table 2 Ratios of heat energy transferred through microregion to the total heat input**

| | $\Theta_{mic}$, W/m | $\Theta_{mac}$, W/m | $\Theta_{mic}/\Theta$,[a] % |
|---|---|---|---|
| $\alpha$ | Ammonia/ethanol | Ammonia/ethanol | Ammonia/ethanol |
| 1.0 | 2.090/0.171 | 3.585/2.184 | 36.82/7.28 |
| 0.7 | 1.904/0.154 | 3.315/2.130 | 36.49/6.76 |
| 0.5 | 1.748/0.133 | 3.098/2.135 | 36.00/5.78 |

[a] $\Theta_{mic} = \int Q_{mic}\, dy$, $\Theta_{mac} = \int Q_{mac}\, dx$, and $\Theta = \Theta_{mic} + \Theta_{mac}$.

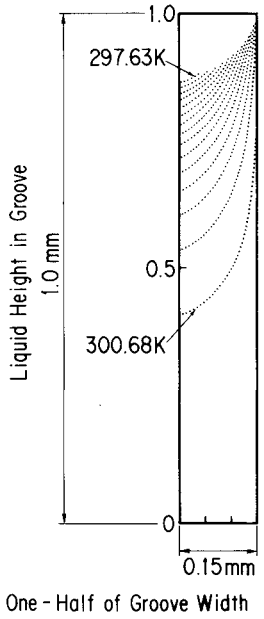


**Fig. 8 Temperature distribution and meniscus contour in the macroregion of ammonia.**

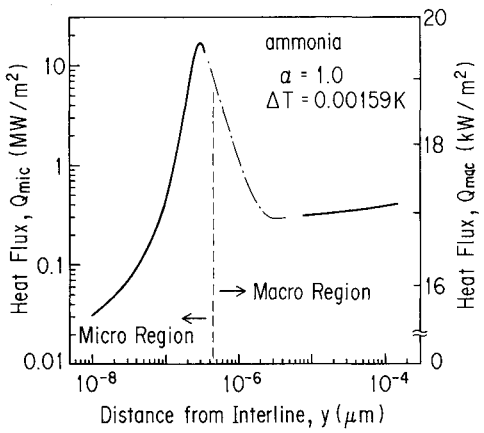


**Fig. 9 Variation of calculated heat flux at the position along a groove wall.**

### B. Experimental Results

Typical film thickness and meniscus configurations measured for ethanol in its vapor environment are shown in Fig. 10, in which the origin of the abscissa shows an arbitrary laser-light-focusing position initially set in the experiment. The surfaces of relatively flat curves in the left half of the figure (called nonevaporative films in this article) were far from smooth and their thicknesses are reduced with increasing heat input to the copper plate. The temperature on the plate changes roughly from 23°C (with no heating) to 80°C (with 700 $W/m^2$ of heat input). The main reason for obtaining such rough surfaces is probably attributed to the measurement accuracy. One source of error lies in the test vessel slider that may generate mechanical vibration in its movement, although all of the optical equipment is set on the air-cushioned optical

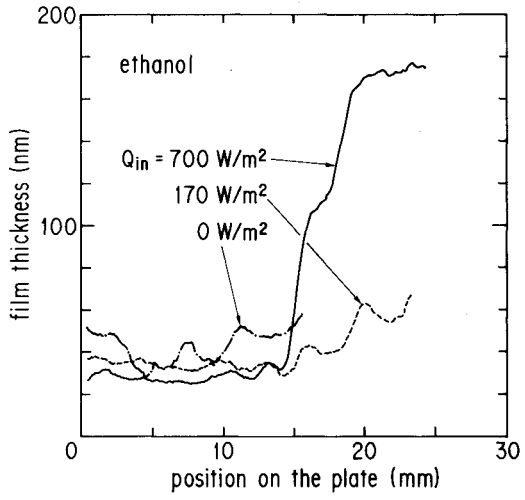


**Fig. 10 Measured film thickness on the inclined copper plate for pure ethanol vapor.**

bench. The second source is the ambiguity in presiding the origin or the starting position of the slider in multiple times of data acquisition processing, which is within $\pm 0.1$ $\mu$m and shall be large enough compared with wavelength of the light. The local temperature distribution on the copper plate as well as roughness of the plate surface may also be involved. The importance of this experiment, however, is that a thin nonevaporative liquid film was measured in the vicinity of meniscus edge at first hand. The average nonevaporative film thickness measured in the case of ethanol vapor was on the order of 30 nm, whereas in the analysis it was several nanometers at most (see Fig. 6). This difference can be explained by the present theory provided that reasonable values for $\alpha$ are incorporated. In comparison to the current analytical result with experimental data of the aforementioned in-house groove heat pipe, the value of $\alpha$ on the order of 0.01 or less would give a film thickness equivalent to those of the experiment, although further investigation is required to determine the value of $\alpha$.

## VI. Concluding Remarks

A local evaporative heat transfer problem at the liquid meniscus edge was theoretically investigated in conjunction with general heat transport relations in the entire flow region. The optical measurement of nonevaporative liquid film thickness was also conducted in order to confirm the assumption used in the theory.

Theoretical results obtained indicate that evaporative heat transfer rates in the groove region are strongly affected by the accommodation coefficient $\alpha$ of working fluid. Theoretical prediction indicates a huge heat transfer rate on the order of MW/m$^2$ can be achieved in a very narrow region less than 1 $\mu$m in width. Accordingly, more than one-third of the total heat energy supplied from the outer surface is transported to the internal vapor core region through the narrow liquid–solid contact region of less than one-hundredth of the total liquid meniscus area in the case of ammonia, whereas in ethanol the role of microregion becomes less significant.

A typical thickness of the nonevaporative liquid film existing in the liquid–solid contact region was in the order of several tens of nanometers by measurement, which can reasonably be explained by the proposed theory when the proper value of $\alpha$ is incorporated.

## References

[1]Bankoff, S. G., "Dynamics and Stability of Thin Heated Liquid Films," *Journal of Heat Transfer*, Vol. 112, 1987, pp. 538–546.

[2]Busse, C. A., and Prenger, F. C., "Numerical Analysis of the Vapour Flow in Cylindrical Heat Pipes," *Research and Development of Heat Pipe Technology, Proceedings of the 5th International Heat Pipe Conference*, edited by K. Oshima, Y. Kobayashi, M. Murakami, and K. Negishi, Japan Association for Heat Pipes, Pt. 1, Tokyo, 1984, pp. 214–219.

[3]Peterson, P. F., and Tien, C. L., "Numerical and Analytical Solution for Two-Dimensional Gas Distribution in Gas-Loaded Heat Pipes," *Journal of Heat Transfer*, Vol. 111, 1989, pp. 598–604.

[4]Faghri, A., "Frozen Start-Up Behavior of Low-Temperature Heat Pipes," *International Journal of Heat and Mass Transfer*, Vol. 35, No. 7, 1992, pp. 1681–1694.

[5]Krishna, R., and Panchal, C. B., "Condensation of a Binary Vapor Mixture in the Presence of an Inert Gas," *Chemical Engineering and Science*, Vol. 32, No. 7, 1977, pp. 741–745.

[6]Peterson, P. F., and Tien, C. L., "Gas-Concentration Measurements and Analysis for Gas-Loaded Thermosyphons," *Journal of Heat Transfer*, Vol. 110, 1988, pp. 743–747.

[7]Kobayashi, Y., Okumura, A., and Matsue, T., "Effect of Gravity and Noncondensable Gas Levels on Condensation in Variable Conductance Heat Pipe," *Journal of Thermophysics and Heat Transfer*, Vol. 5, No. 1, 1991, pp. 61–68.

[8]Berger, M. E., and Feldman, K. T., Jr., "Analysis of Circumferentially Grooved Heat Pipe Evaporators," American Society of Mechanical Engineers Paper 73-WA/HT-13, 1974.

[9]Derjaguin, B. V., and Zorin, Z. M., "Optical Study of the Adsorption and Surface Condensation of Vapours in the Vicinity of Saturation on a Smooth Surface," *Proceedings of the 2nd International Congress of Surface Activity*, London, Vol. 2, 1957, pp. 145–152.

[10]Potash, M., Jr., and Wayner, P. C., Jr., "Evaporation from a Two-Dimensional Extended Meniscus," *International Journal of Heat and Mass Transfer*, Vol. 15, Pergamon, 1972, pp. 1851–1863.

[11]Wayner, P. C., Jr., "Adsorption and Capillary Condensation at the Contact Line in Change of Phase Heat Transfer," *International Journal of Heat and Mass Transfer*, Vol. 25, No. 5, 1982, pp. 707–713.

[12]Wehrle, V. A., and Voulelikas, G., "Evaporation from Two-Dimensional Meniscus," *AIAA Journal*, Vol. 23, No. 2, 1985, pp. 309–313.

[13]Mirzamoghadam, A., and Catton, I., "A Physical Model of the Evaporating Meniscus," *Journal of Heat Transfer*, Vol. 110, 1988, pp. 201–207.

[14]Stephan, P. C., and Busse, C. A., "Analysis of the Heat Transfer Coefficient of Grooved Heat Pipe Evaporator Walls," *International Journal of Heat and Mass Transfer*, Vol. 35, No. 2, 1992, pp. 383–391.

[15]Kobayashi, Y., Toyokawa, S., and Araki, T., "Heat and Mass Transfer from Thin Liquid Film in the Vicinity of the Interline of Meniscus," *Thermal Science and Engineering*, Vol. 2, No. 1, 1994, pp. 45–51.

[16]Hirata, K., et al. (ed.), *JSME Data Book: Thermophysical Properties of Fluids*, JSME Publishing, Tokyo, 1983 (in Japanese).